Toward Dexterous Manipulation With Augmented Adaptive Synergies: The Pisa/IIT SoftHand 2

Cosimo Della Santina, Cristina Piazza, Giorgio Grioli, Manuel G. Catalano, and Antonio Bicchi, *Fellow, IEEE*

***Abstract*—In recent years, a clear trend toward simplification emerged in the development of robotic hands. The use of soft robotic approaches has been a useful tool in this prospective, enabling complexity reduction by embodying part of grasping intelligence in the hand mechanical structure. Several hand prototypes designed according to such principles have accomplished good results in terms of grasping simplicity, robustness, and reliability. Among them, the Pisa/IIT SoftHand demonstrated the feasibility of a large variety of grasping tasks, by means of only one actuator and an opportunely designed tendon-driven differential mechanism. However, the use of a single degree of actuation prevents the execution of more complex tasks, like fine preshaping of fingers and in-hand manipulation. While possible in theory, simply doubling the Pisa/IIT SoftHand actuation system has several disadvantages, e.g., in terms of space and mechanical complexity. To overcome these limitations, we propose a novel design framework for tendon-driven mechanisms, in which the main idea is to turn transmission friction from a disturbance into a design tool. In this way, the degrees of actuation (DoAs) can be doubled with little additional complexity. By leveraging on this idea, we design a novel robotic hand, the Pisa/IIT SoftHand 2. We present here its design, modeling, control, and experimental validation. The hand demonstrates that by opportunely combining only two DoAs with hand softness, a large variety of grasping and manipulation tasks can be performed, only relying on the intelligence embodied in the mechanism. Examples include rotating objects with different shapes, opening a jar, and pouring coffee from a glass.**

***Index Terms*—Biologically inspired robots, dexterous manipulation, mechanism design, multifingered hands, underactuated robots.**

Manuscript received November 6, 2017; accepted March 20, 2018. Date of publication June 6, 2018; date of current version October 2, 2018. This paper was recommended for publication by Associate Editor S. Hirai and Editor A. Billard upon evaluation of the reviewers' comments. This work was supported by the European Unions Horizon 2020 Research and Innovation Program under Grant Agreement 645599 (Soma) and 688857 (SoftPro). *(Corresponding author: Cosimo Della Santina.)*

C. Della Santina and C. Piazza are with the Research Center "Enrico Piaggio," University of Pisa, Pisa 56126, Italy (e-mail: cosimodellasantina@gmail.com; cristina.piazza@ing.unipi.it).

G. Grioli and M. G. Catalano are with Soft Robotics for Human Cooperation and Rehabilitation, Istituto Italiano di Tecnologia, Genova 16163, Italy (e-mail: giorgio.grioli@gmail.com; manuel.catalano@iit.it).

A. Bicchi is with the Research Center "Enrico Piaggio," University of Pisa, Pisa 56126, Italy, and also with the Soft Robotics for Human Cooperation and Rehabilitation, Istituto Italiano di Tecnologia, Genova 16163, Italy (e-mail: antonio.bicchi@unipi.it).

This paper has supplementary downloadable material available at http://ieeexplore.ieee.org.

Color versions of one or more of the figures in this paper are available online at http://ieeexplore.ieee.org.

Digital Object Identifier 10.1109/TRO.2018.2830407

I. Introduction

NOTWITHSTANDING the many advances, designing dexterous robotic hands remains one of the biggest challenges in robotics. Over the years, several design methods and prototypes have been proposed. One approach followed by many researchers consists in attempting to closely replicate the features of human hands with sophisticated designs integrating many actuators and sensors (e.g., [1]–[3]). A second approach, followed mostly by designers of gripping devices for industrial or prosthetic applications, consists in developing nonanthropomorphic, simple and rugged devices, designed on purpose to solve a restricted class of tasks (e.g., [4]–[7]). A third trend aspires to make hands retaining advantages of the anthropomorphic design, while drastically reducing complexity in terms of number of actuators, sensors, and lines of code to program the control. One of the most effective and widely used tools for mechanical simplification is underactuation [8], by which designers can reduce the number of degrees of actuation (DoAs) of robotic hands while maintaining a large number of degrees of freedom (DoFs). Notable examples of this line of research are [9]–[13].

In this regard, principles from human motor control are often used as inspiration to guide hand design. Postural synergies are a valuable example of this approach. They specify a reduced set of principal directions in hand configuration space, describing the most commonly observed postures in human hand movements [14]. By constraining the motion of artificial hands along these directions, simplification in programing [15] and design [16] can be achieved. However, a rigidly prescriptive, purely geometric model of synergies was recognized to be not ideal for describing the extremely adaptive nature of human hands in grasping and manipulating objects. In the *soft synergy* model [17], the issue is addressed by considering postural synergies as only prescribing motion of a virtual reference hand toward which the physical hand is dynamically attracted. The actual hand posture emerges as an equilibrium between environment resistance to penetration and hand compliance. In [18], some of the authors of the present paper showed that a system of differential transmissions and compliant elements can be designed so as to implement a combination of any number of soft synergies. The idea of designing force distribution mechanisms that replicate the soft synergy model was called *adaptive synergies*. Its application brought to the development of Pisa/IIT SoftHand [19] [see Fig. 3(a)], an anthropomorphic robotic hand implementing one soft synergy. Even with such a small actuation

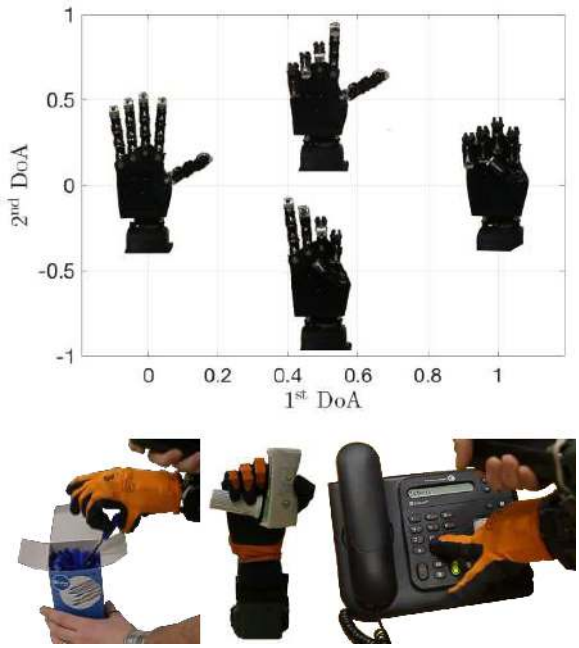

Fig. 1. Pisa/IIT SoftHand 2 is a novel anthropomorphic robotic hand. It implements two DoAs in a compact design, thanks to a mechanism that exploits frictional effects. The hand-free motions shown in the top part of the figure are designed so to resemble the main natural postural synergies. As a result, the Pisa/IIT SoftHand 2 combines good grasping performance and dexterous in-hand manipulation capabilities. A few examples are depicted in the bottom. Here, the hand performs a pinch grasp, a power grasp of multiple objects, and it pushes a button by using the extended index.

space, the hand was able to realize a vast range of grasps, thanks to its physical adaptiveness and compliance.

However, while very effective in many practical conditions, Pisa/IIT SoftHand presents obvious limitations in terms of dexterity if compared to its natural counterpart. So, facing the need of augmenting the dexterity of these kind of simple hands, the following problem arises: how to increase the hand functionalities without sensibly increasing mechanical complexity?

This paper deals with this complexity–dexterity tradeoff by proposing a novel framework for the design of tendon driven underactuated hands, which, in continuity with our previous work, we will refer to as *augmented adaptive synergies*. The main idea behind this approach is to exploit friction effects to generate extra motions with minimal changes in the original mechanics. Using this approach, we present the design and validation of a novel self-contained robotic hand, named Pisa/IIT SoftHand 2 (called hereinafter SoftHand 2). This novel hand is able to perform both precision and power grasps (see Fig. 1), as well as to manipulate objects while maintaining a stable grasp through autonomous finger motions dictated by its mechanical intelligence. Note that to implement in-hand manipulation in fully actuated hands, sophisticated algorithms [20]–[22] and sensing strategies [23] are generally required. In contrast, SoftHand 2 can manipulate objects of different shapes with just two DoAs, and requires only a very simple control strategy.

The paper is organized as follows. After recalling the main elements of the adaptive synergy framework in Section II, we introduce and discuss the augmented adaptive synergies framework in Section III for a generic tendon-driven mechanism. Section IV presents SoftHand 2 mechanical design. In Section V, we derive a dynamical model of the proposed hand, to perform simulations motivating the considered control policy and corroborating the analytical results. SoftHand 2 performance are tested through several experiments in Section VI. The present paper extends [24], where the proposed actuation principle was preliminarily introduced and implemented in an exploratory prototype.

II. Background

The simplest definition of *postural synergies* is an ordered basis of the vector space of joint variables $q \in \mathbb{R}^n$, resulting from principal component analysis of the covariance matrix obtained from experimental measurements of human subjects during normal hand use [25]. The eigenvectors of the covariance matrix ordered by their eigenvalues form the columns of the *synergy* matrix S, so that it holds

$$q = S\sigma \tag{1}$$

where $\sigma \in \mathbb{R}^{n_s}$ represents the posture in the synergy basis $S \in \mathbb{R}^{n \times n_s}$. While the complete description of the joint space would require $n_s = n$, experimental evidence suggest that a reduced basis is sufficient to explain a large part of the covariance of grasp postures during common grasping tasks [25]. These experiments however were conducted while subjects mimed grasp, without physically interacting with objects, as hand deformations due to contact forces would confound results. As a consequence, the synergy model in (1) is adequate to describe preshaping phases of grasp, but fails to predict how grasping forces are actually generated in contact.

To address this issue, [17] proposed to use the synergy model to generate reference motions for the hand. It also introduced a model of compliance of the hand to account for forces arising from resistance to interpenetration of bodies. This *soft synergy* model postulates that under such attraction and repulsion forces, the hand reaches the equilibrium configuration described by

$$q = S\sigma - CJ^T f_{\text{ext}} \tag{2}$$

where C represents the grasp compliance and the term $J^T f_{\text{ext}}$ collects all contact forces acting on the hand (see Fig. 2).

Due to technological difficulties, the realization of an artificial hand implementing the model (2) was not obtained directly. Instead, Grioli *et al.* [18] introduced the design technique of adaptive synergies, which exploits differential mechanisms and the space of self-motions to adapt to the external world. For a hand, which is actuated by means of t tendons connected to as many motors through a differential mechanism with transmission distribution matrix R, one can write a relation between the tendon positions $x \in \mathbb{R}^t$ and joint variables as

$$Rq = x \tag{3}$$

and, by kineto-static duality, infer

$$\tau = R^T \tau_M \tag{4}$$

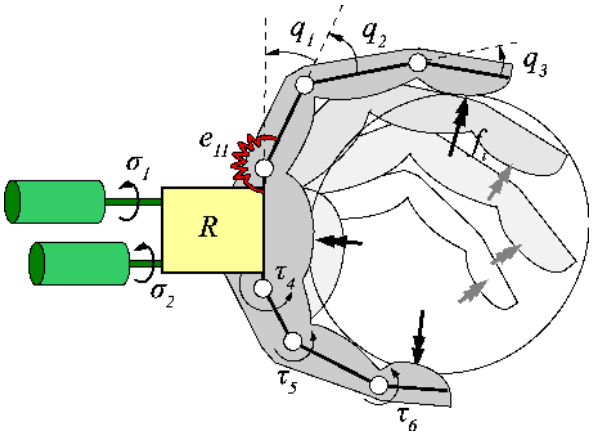

Fig. 2. Schematic of a robotic hand with adaptive synergies grasping an object. The prime movers, on the left (in green) generate motion acting on the angles σ. Those motions are mapped to the hand joint angles q through the matrix R, which collects the transmission ratios. The final posture of the hand depends on the external wrenches $f_{\text{ext}} = [f_1^T, f_2^T, \ldots]^T$, the internal torques $\tau_a = [\tau_1, \tau_2, \ldots]^T$, and the springs elasticity (matrix E collects all the stiffness in its elements $e_{i,j}$).

where τ is the joint torque vector and τ_M is the tendon tension vector. The equilibrium of the joint torques is obtained by including a linear elastic force in joint space $(-Eq)$, and the contribution of external forces $(J^T f_{\text{ext}})$

$$J^T f_{\text{ext}} = R^T \tau_M - Eq\,. \tag{5}$$

Finally, combining (3) and (5) and solving yields

$$\begin{aligned} q = {} & (-E^{-1} + E^{-1}R^T(RE^{-1}R^T)^{-1}RE^{-1})J^T f_{\text{ext}} \\ & + E^{-1}R^T(RE^{-1}R^T)^{-1}x \end{aligned} \tag{6}$$

which can be made equivalent to the soft synergies (2) by identifying the tendon position with the synergy reference variable (i.e., $x = \sigma$), and by properly designing the parameters in R and E so that

$$\begin{aligned} S &= E^{-1}R^T(RE^{-1}R^T)^{-1} = R_E^+ \\ C &= E^{-1} - E^{-1}R^T(RE^{-1}R^T)^{-1}RE^{-1} = P_R^{\perp}E^{-1}. \end{aligned} \tag{7}$$

This method was used for the design of the Pisa/IIT SoftHand [see Fig. 3(a)], where the differential mechanism is obtained using a single motor (i.e., $t = 1$), which actuates all joints at the same time through a tendon. The physical parameters were chosen such as to implement the first soft synergy of grasp [25]. With the same method, it is possible to add more synergies to the hand by adding other tendons in parallel to the first one. As a proof of concept of multisynergy hands, a prototype was presented in [18] [see Fig. 3(b)]. However, multisynergies hands require multiple tendons to be independently routed through all hand joints, hence a large number of pulleys and an overall increase in size, weight, and complexity.

III. Augmented Adaptive Synergies

A. From Friction Effects to Actuation Augmentation

The ideal model presented in Section II does not account for dissipative effects that are encountered in any real mechanism.

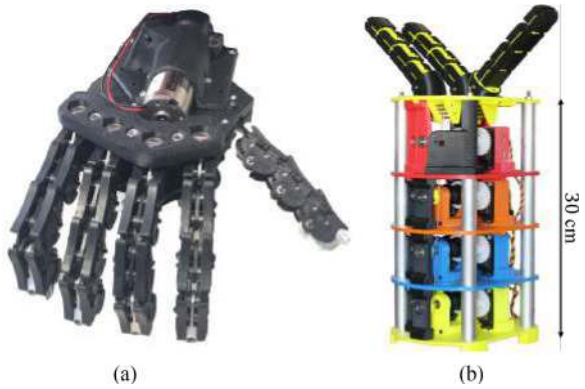

Fig. 3. Robotic hands designed through adaptive synergies: Pisa/IIT SoftHand integrates one DoA in a compact setup, while the second hand implements four synergies at the cost of a cumbersome structure. (a) Original Pisa/IIT SoftHand. (b) Second hand.

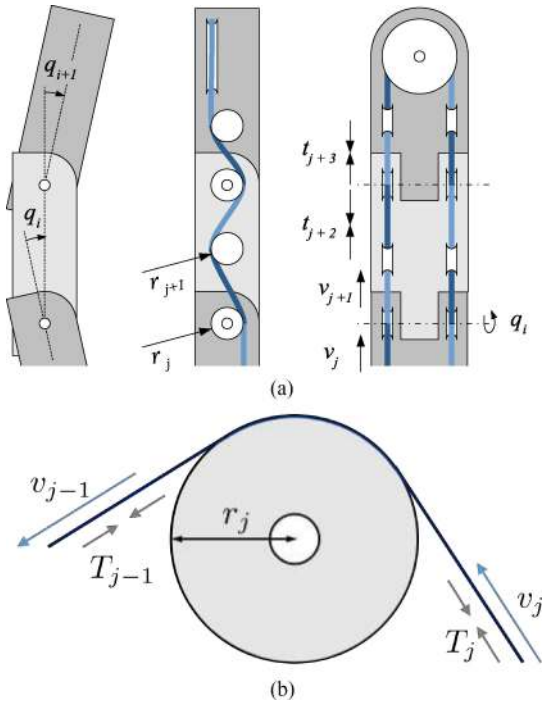

Fig. 4. Panel (a) presents the scheme of an adaptive finger actuated through a tendon, with main variables highlighted. Panel (b) shows a portion of the mechanism. It is composed by two tendon segments, and the pulley that separates them. q_i is the ith joint angle, v_j and T_j are the speed and tension, respectively, of each segment of the tendon along its routing, $r_{j,i}$ is the radius r_j of the jth pulley when it is on joint i, or 0 otherwise. (a) Finger. (b) Pulley.

Fig. 4(a) shows a sketch of a robotic finger, driven by a unique tendon, with significant quantities marked. In a tendon-driven differential mechanism, one of the main sources of nonlinearity is the friction generated by pulleys guiding the tendon throughout the hand transmission system.

To mathematically describe the effects of friction, we consider the $m + 1$ tendon segments, delimited by the m pulleys. We assume inextensible tendons, and thus constant speed and tension within each segment. Let T_j and v_j be the tension and speed of the jth segment, and $v \in \mathbb{R}^{m+1}$ and $T \in \mathbb{R}^{m+1}$ be the two vectors collecting these terms. We refer to the jth pulley

radius as r_j. To write compact expressions in the following, we also define $r_{i,j}$ as the radius r_j of the jth pulley, if the pulley is part of joint i, i.e., if a change in q_i is reflected in a change of the length of the jth segment. The value of $r_{i,j}$ is zero otherwise. Fig. 4(b) shows the jth portion of the transmission mechanism, composed by two successive tendon segments, and the pulley which separates them. By balancing velocities at jth pulley, we obtain m equations in $m+1$ unknowns, in the form

$$v_j = v_{j-1} + \frac{\mathrm{d}l_j(q)}{\mathrm{d}t} = v_{j-1} + \sum_{i=1}^{n} r_{j,i}\,\dot{q}_i \tag{8}$$

where v_j is the velocity of the jth segment, and $l_j(q)$ its length. Note that the length of the segment changes only if it passes through a joint. In that case, a variation of joint angle is reflected in a proportional variation of the segment length.

We complete the velocity balance through a boundary equation defined as

$$\dot{s} = -\frac{v_0 + v_m}{2} \tag{9}$$

where v_0 and v_m are the velocities of first and last segments of the tendon, and $\dot{s}$ is the residual sliding speed. Note that the variable s is an extra degree of freedom independent from the joint angles q, which describes the relative motion of the two ends of the tendon. Consider indeed that when all the DoFs of the hand are constrained (i.e., $\dot{q} \equiv 0$), the tendon can still slide along its path, being all pulleys idle.

Analogous considerations can be done for the balance of tensions at the jth pulley

$$T_j = T_{j-1} - V_j(v_j) \tag{10}$$

where T_j is the tension on the jth segment. The tension loss $V_j(v_j)$ is due to friction on the jth pulley. We complete the tension balances through the $m+1$th equation

$$\tau_M = T_0 + T_m \tag{11}$$

which accounts for the total pulling force τ_M applied by the motor on the synergy σ. T_0 and T_m are the tensions of first and last portions of the tendon.

Finally, we impose the map between tensions and joint torques, i.e.,

$$\tau_i = -\sum_{j=1}^{m+1} r_{j,i} T_j \tag{12}$$

where $r_{j,i}$ is defined as in (8), and τ_i is the torque applied by the tendon on the ith joint.

We rewrite the previous equations in matrix form as

$$\begin{cases} MT + V(v) + e\tau_M = 0 \\ Mv - \bar{R}\dot{q} = -2e\dot{s} \\ \tau = -\bar{R}^T T \end{cases} \tag{13}$$

where $M \in \mathbb{R}^{m+1\times m+1}$, $\bar{R} \in \mathbb{R}^{n\times m+1}$, and $e = [0, 0, \ldots, 0, 1]^T \in \mathbb{R}^{m+1}$. Note that the element (j,i) of $\bar{R}$ is $r_{j,i}$. Note also that $V(v)$ is a vector function, with jth element $V_j(v_j)$.

From (13), we explicit the velocity and tension distributions v and T as

$$\begin{cases} v &= +M^{-1}\bar{R}\dot{q} - 2\,e_v\dot{s} \\ T &= -M^{-1}V(v) - M^{-1}e\tau_M = -M^{-1}V(v) + e_v\tau_M \end{cases} \tag{14}$$

where $e_v = -M^{-1}e = [1, 1, \ldots 1, 1]^T$. Combining (14) with the third equation in (13), the overall relation between $\dot{s}$, τ_{M}, and joint torque vector τ yields

$$\begin{aligned} \tau &= -\bar{R}^T(-M^{-1}V(M^{-1}\bar{R}\dot{q} - e_v\dot{s}) + e_v\tau_{\mathrm{M}}) \\ &= R^T\,\tau_M + D(\dot{q}, \dot{s}) \end{aligned} \tag{15}$$

where we defined the transmission maps as

$$\begin{cases} R^T = -\bar{R}^T e_v \\ D(\dot{q}, \dot{s}) = -\bar{R}^T(-M^{-1}V(M^{-1}\bar{R}\dot{q} - 2\,e_v\dot{s})). \end{cases} \tag{16}$$

Equation (15) clearly introduces the possibility of using tendon sliding $\dot{s}$ as an actuation, with the nonlinear input field $D(\dot{q}, \dot{s})$. This is in addition to the input τ_M mapped as in (4), de facto doubling the amount of DoA realized by each tendon.

To simplify the transmission model $D(\dot{q}, \dot{s})$, it is instrumental to define a specific model for the friction force $V(v)$. Consider initially a dynamic Coulomb-like friction model (as, e.g., described in [26])

$$V(v) = V_{\max}\tanh(v) = V_{\max}\tanh(M^{-1}\bar{R}\dot{q} - e_v\dot{s}) \tag{17}$$

where $\tanh(\cdot)$ is intended component-wise for vectors. In Section V-A, we discuss different friction models. Assuming the system in equilibrium (i.e., $\dot{q} \equiv 0$), and considering $e_v = [1, 1 \ldots 1]^T$, (16) yields

$$\begin{aligned} D(\dot{s}) &= -\bar{R}^T(M^{-1}V_{\max}\,\tanh(2e_v\dot{s})) \\ &= -\bar{R}^T M^{-1}V_{\max}\,e_v\tanh(2\dot{s}). \end{aligned} \tag{18}$$

Introducing (15) and (18) in the force balance (5), we obtain

$$J^T f_{\text{ext}} = R^T u_1 + R_f^T u_2 - Eq \tag{19}$$

where $u_1 = \tau_M$, $u_2 = \tanh(2\dot{s})$, and

$$\begin{cases} R^T = -\bar{R}^T e_v \\ R_f^T = -\bar{R}^T M^{-1}V_{\max}e_v\ . \end{cases} \tag{20}$$

In analogy to Section II, we define a synergy-like input σ_f

$$\begin{cases} Rq = \sigma \\ R_f q = \sigma_f. \end{cases} \tag{21}$$

Rewriting (19) and (21) in matrix form, we obtain

$$\begin{bmatrix} -E & [R^T\ R_f^T] \\ \begin{bmatrix} R \\ R_f \end{bmatrix} & \emptyset \end{bmatrix} \begin{bmatrix} q \\ \begin{bmatrix} u_1 \\ u_2 \end{bmatrix} \end{bmatrix} = \begin{bmatrix} J^T f_{\text{ext}} \\ \begin{bmatrix} \sigma \\ \sigma_f \end{bmatrix} \end{bmatrix} \tag{22}$$

where the left-term matrix is always nonsingular. Through block inversion, the solution of (22) can be written as

$$q = \begin{bmatrix} R \\ R_f \end{bmatrix}_E^+ \begin{bmatrix} \sigma \\ \sigma_f \end{bmatrix} + P_{R,Rf}^{\perp} E^{-1} J^T f_{\text{ext}} \tag{23}$$

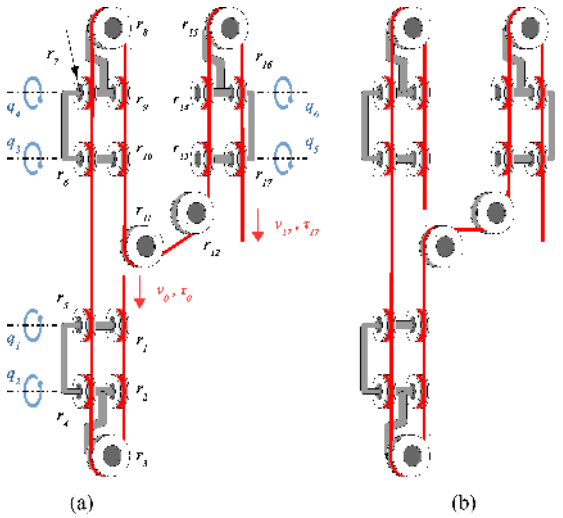

Fig. 5. Simple adaptive hand with main quantities highlighted. q_i is the ith joint angle. v_0, v_{17} and T_0, T_{17} are the speed and the tension at the two ends of the tendon. r_i is the radius of the ith pulley. We consider here two possible routings, i.e., orders in which the tendon passes through pulleys. (a) Routing 1. (b) Routing 2.

which explicitly specifies the relationship between synergistic inputs and hand configurations, supporting our proposed idea to exploit friction to enhance the controllability of the hand.

B. Effect of Routing Changes

We consider here the possibility of changing the routing of the tendon, i.e., the order by which the tendon passes through pulleys, as an additional design parameter to shape the hand closure. Fig. 5 shows an example of two hands with the same structure but different routing.

To describe the routing, we introduce the permutation matrix $P \in \mathbb{R}^{m+1\times m+1}$. Its rows identify the hand pulleys, and the columns identify the tendon portions. $P_{i,j} = 1$ if the jth portion of the tendon is driven by the ith pulley, $P_{i,j} = 0$ otherwise. All the derivations of the previous section can be generalized by substituting v and T with their reorganized counterparts Pv and PT, respectively. Thus, the overall effect is to modify (13), into

$$\begin{cases} M\,P\,T + V(P\,v) + e\tau_{\mathrm{M}} = 0 \\ M\,P\,v - \bar{R}\dot{q} = -2e\dot{s} \\ \tau = -\bar{R}^T\,PT\,. \end{cases} \tag{24}$$

The two directions of actuation R, R_f become

$$\begin{cases} R^T = -\bar{R}^T e_v \\ R_f^T = -\bar{R}^T\,PM^{-1}P^T V_{\max} e_v\ . \end{cases} \tag{25}$$

It is worth noticing that the effect of a different routing reflects just in a change of the second direction of actuation R_f, leaving R unchanged.

C. Design Remarks

The method of *Adaptive Synergies* [19] was motivated by the idea of using (7) for designing parameters R, E such that a desired synergy basis S could be obtained. Here, we extended this method including the possibility of designing also the friction parameters in $V_{\max}$ and the tendon routing P. To clarify the *Augmented Adaptive Synergies* approach, consider the simple example of Fig. 5; a hand with three fingers. This hand has a total of 6 joints and 17 pulleys. They divide the tendon into 18 segments, each with constant velocity and tension. T, v, q, respectively, are tensions, velocities, and joint angles vectors

$$T = \begin{bmatrix} T_1 \\ \vdots \\ T_{18} \end{bmatrix}, \quad v = \begin{bmatrix} v_1 \\ \vdots \\ v_{18} \end{bmatrix}, \quad q = \begin{bmatrix} q_1 \\ \vdots \\ q_6 \end{bmatrix}. \tag{26}$$

We start by considering the routing in panel (a), which corresponds to a P equal to the identity. So to describe hand structure, we specify the following the matrices in (13). Independently from the hand structure, M presents the form

$$M = \begin{bmatrix} -1 & 1 & 0 \dots & 0 & 0 \\ 0 & -1 & 1 \dots & 0 & 0 \\ \vdots & \vdots & \vdots \ddots & \vdots & \vdots \\ 0 & 0 & 0 \dots & -1 & 1 \\ 1 & 0 & 0 \dots & 0 & 1 \end{bmatrix} \in \mathbb{R}^{18\times 18}. \tag{27}$$

The two matrices incorporating hand structure are $\bar{R}$ and $V_{\max}$. The transmission between tendon and joints is described by the matrix

$$\bar{R} = \begin{bmatrix} \bar{R}_1 & \emptyset & \emptyset \\ \emptyset & \bar{R}_2 & \emptyset \\ \emptyset & \emptyset & \bar{R}_3 \\ \bar{0} & \bar{0} & \bar{0} \end{bmatrix} \in \mathbb{R}^{18\times 6} \tag{28}$$

with

$$\bar{R}_1 = \begin{bmatrix} r_1 & 0 \\ 0 & r_2 \\ 0 & 0 \\ 0 & r_4 \\ r_5 & 0 \end{bmatrix} \quad \bar{R}_2 = \begin{bmatrix} r_6 & 0 \\ 0 & r_7 \\ 0 & 0 \\ 0 & r_9 \\ r_{10} & 0 \end{bmatrix} \quad \bar{R}_3 = \begin{bmatrix} 0 & 0 \\ 0 & 0 \\ r_{13} & 0 \\ 0 & r_{14} \\ 0 & 0 \\ 0 & r_{16} \\ r_{17} & 0 \end{bmatrix} \tag{29}$$

where $\emptyset$ is a zero matrix and $\bar{0}$ is a zero vector of opportune dimensions. The block $\bar{R}_i$ refers to the ith finger, and it contains the radii of the pulleys acting on that finger joints. The friction effects matrix $V_{\max}$ has the diagonal form

$$V_{\max} = \begin{bmatrix} V_1 & 0 \dots & 0 & 0 \\ 0 & V_2 \dots & 0 & 0 \\ \vdots & \vdots \ddots & \vdots & \vdots \\ 0 & 0 & V_{17} & 0 \\ 0 & 0 & 0 & 0 \end{bmatrix} \in \mathbb{R}^{18\times 18} \tag{30}$$

where V_i is the friction coefficient associated with the ith pulley. Note that the last row of $\bar{R}$, $V_{\max}$, and M reflect (9) and (11). From (20), we obtain the vectors R, R_f representing the two

directions of actuation

$$R^T = \begin{bmatrix} r_1 + r_5 \\ r_2 + r_4 \\ r_6 + r_{10} \\ r_7 + r_9 \\ r_{13} + r_{17} \\ r_{14} + r_{16} \end{bmatrix} \tag{31}$$

$$R_f^T = \begin{bmatrix} \frac{r_1 - r_5}{2} \sum_{i=1}^{4} V_i + \frac{r_1 + r_5}{2} \sum_{i=5}^{17} V_i \\ \frac{r_2 - r_4}{2} \sum_{i=2}^{3} V_i + \frac{r_2 + r_4}{2} \left(\sum_{i=4}^{17} V_i - V_1 \right) \\ \frac{r_6 - r_{10}}{2} \sum_{i=6}^{9} V_i + \frac{r_6 + r_{10}}{2} \left(\sum_{i=10}^{17} V_i - \sum_{i=1}^{5} V_i \right) \\ \frac{r_7 - r_9}{2} \sum_{i=7}^{8} V_i + \frac{r_7 + r_9}{2} \left(\sum_{i=9}^{17} V_i - \sum_{i=1}^{6} V_i \right) \\ \frac{r_{13} - r_{17}}{2} \sum_{i=13}^{16} V_i + \frac{r_{13} + r_{17}}{2} \left(V_{17} - \sum_{i=1}^{12} V_i \right) \\ \frac{r_{14} - r_{16}}{2} \sum_{i=14}^{15} V_i + \frac{r_{14} + r_{16}}{2} \left(\sum_{i=16}^{17} V_i - \sum_{i=1}^{13} V_i \right) \end{bmatrix}. \tag{32}$$

From (31), it is clear that R can be designed through the choice of pulley radii semisum. Additionally, (32) shows that R_f can be shaped independently from R through pulley radii semidifferences and friction coefficients. We consider here equal pulley radii, friction, and elastic effects, i.e., $r_i = \bar{r}$, $V_i = \bar{V}\ \forall i$, and $E = k\,I$. From (23), the free-closure configuration space is

$$\text{Span} \left\{ \begin{bmatrix} 1 \\ 1 \\ 1 \\ 1 \\ 1 \\ 1 \end{bmatrix}, \begin{bmatrix} 17 \\ 17 \\ 2 \\ 2 \\ -19 \\ -19 \end{bmatrix} \right\}. \tag{33}$$

The first direction is a coordinate closure of all angles, while the second one corresponds roughly to a closure of the first finger and an opening of the third, or vice versa.

As an example of independent design of closure directions, we change the friction on pulley 11 (i.e., $V_{11} = \alpha\,\bar{V}$) and the semidifference of pulley radii acting on the joint q_3 (i.e., $r_6 = \bar{r} + \beta$ and $r_{10} = \bar{r} - \beta$). The resulting free-closure configuration space is

$$\text{Span} \left\{ \begin{bmatrix} 1 \\ 1 \\ 1 \\ 1 \\ 1 \\ 1 \end{bmatrix}, \begin{bmatrix} 16 \\ 16 \\ 1 \\ 1 \\ -17 \\ -17 \end{bmatrix} + \alpha \begin{bmatrix} 1 \\ 1 \\ 1 \\ 1 \\ -2 \\ -2 \end{bmatrix} + \frac{\beta}{r} \begin{bmatrix} -1 \\ -1 \\ 5 \\ -1 \\ -1 \\ -1 \end{bmatrix} \right\} \tag{34}$$

where $\alpha \in (0, +\infty)$, $\beta \in (-\bar{r}, +\bar{r})$. Hence, we can use friction to modulate differences in closure between one finger and the others, and radii variations to modulate joint closure on a same finger.

Fig. 6. Pisa/IIT SoftHand 2 evolves Pisa/IIT SoftHand through the introduction of an additional DOA, powered by a friction-based transmission system. The hand design is self-contained, including the whole actuation system, sensors, power, and control electronics.

To clarify the effect of a routing change, we consider the routing in Fig. 5(b). The corresponding matrix P is

$$P = \begin{bmatrix} \emptyset & \Pi_{5\times 5} & \emptyset \\ \Pi_{5\times 5} & \emptyset & \emptyset \\ \emptyset & \emptyset & I_{8\times 8} \end{bmatrix} \tag{35}$$

where each block represents a finger, $I_{8\times 8} \in \mathbb{R}^{8\times 8}$ is the identity matrix, and $\Pi_{5\times 5} \in \mathbb{R}^{5\times 5}$ is the matrix with all zero elements except to the ones on the antidiagonal (i.e., $\Pi_{i,6-i} = 1\ \forall\, i \in \{1 \dots 5\}$, and 0 otherwise).

Hence, from (25), tacking equal pulleys and elastic effects (i.e., $r_i = \bar{r}$, $V_i = \bar{V}\ \forall i$, $E = k\,I$), the following free closure configuration space results:

$$\text{Span} \left\{ \begin{bmatrix} 1 \\ 1 \\ 1 \\ 1 \\ 1 \\ 1 \end{bmatrix}, \begin{bmatrix} 2 \\ 2 \\ 17 \\ 17 \\ -19 \\ -19 \end{bmatrix} \right\}. \tag{36}$$

Thus, the net effect of this routing change is to leave the first direction unchanged, and to modify the second, reorganizing its elements.

IV. Augmented Synergy Driven Hand: The Pisa/IIT SoftHand 2

We present here the Pisa/IIT SoftHand 2, an anthropomorphic robotic hand evolving the Pisa/IIT SoftHand by the introduction of a friction mediated DoA. Fig. 6 shows the hand prototype, while Fig. 7(a) shows a sketch of the transmission system. Pisa/IIT SoftHand 2 has 19 joints. Five of them are simple revolute joints, and they implement the adduction/abduction movement of each finger. The remaining 14 joints are compliant rolling-contact element (CORE) joints [27] (see appendix A for more details). This choice strongly increases the hand

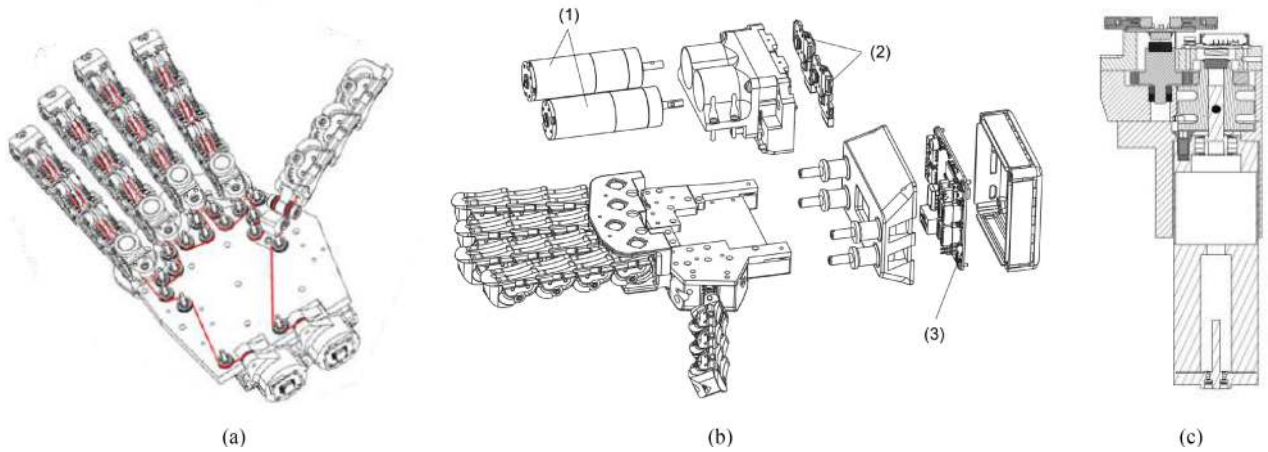

Fig. 7. Sketches of SoftHand 2 prototype. The red line in panel (a) highlights the tendon route. Panel (b) presents main components of SoftHand 2: (1) are the two motors, (2) are the four encoders, (3) is the control and power electronics. Panel (c) reports a 2-D section of the motor and encoder assembly. (a) Routing. (b) Exploded sketch. (c) Motor and encoder.

robustness, such as the similarity between its kinematics and one of the human hands. Elasticity is introduced in each joint as discussed in Appendix B. A single tendon moves from the palm base, through all the fingers. Two motors actuate the tendon, pulling it from its two sides. If the motors move in the same direction, the tendon length is shortened, and the SoftHand 2 closes. This corresponds to a σ command in (23). If instead the two motors move in opposition, the tendon slides (i.e., $\dot{s} \neq 0$), and the hand moves according to the friction-driven DoA. This corresponds to a σ_f command in (23). Fig. 1 graphically represents these two DoAs.

These two free closures are designed through the proposed augmented adaptive synergies framework. Their choice is motivated by a tradeoff between human inspiration and simplicity of implementation. For the closure related to the first degree of actuation σ, we target a coordinate closure of all fingers analogous to the first synergy of grasp in humans [25]. This seems to be a very fundamental ingredient of human hand control, since the same synergy was discovered during analysis of haptic exploration [28] and environmental constraint exploitation [29]. For the second DoA, we target a behavior similar to the one extensively described in the toy example of Section III-C. Indeed, the relative opening and closing of left fingers w.r.t. right ones (and vice versa) is found in the second and third postural synergies of grasp [25], [30], in the second manipulation synergy in [31], in the second synergy of haptic exploration [28], and in the third synergy of environmental constrain exploitation in [29]. So the intuition that we follow here is that the implementation of a similar motion could be a key ingredient for embedding a higher level of dexterous capabilities. This was tested in extensive experiments, presented in Section VI.

We designed custom pulleys with equal radii 3.5 mm. All are made of the same material, with a friction constant approximately of $\bar{v} \simeq 0.3 \frac{\mathrm{N}}{\mathrm{mm}}$ [32]. We made the elastic elements of natural rubber with the addition of carbon black, to obtain $k \simeq 1.2 \frac{\mathrm{N}}{\mathrm{mm}}$. Neglecting the four long fingers abduction joints (see Section V for more details) and considering a linear elastic field, the input directions of the two DoAs results from (20) as the span of $[1, \ldots, 1]^{\mathrm{T}}\mathrm{N}$ and $[33, 33, 33, 17, 17, 17, 1, 1, 1, -15, -15, -15, -31, -31, -31]^{\mathrm{T}}\mathrm{N}$. As prescribed by (23), the free-closure configuration space is the span of $[1, \ldots, 1]^{\mathrm{T}}$ and $[2, 2, 2, 1, 1, 1, 0, 0, 0, -1, -1, -1, -2, -2, -2]^{\mathrm{T}}$, compatibly with physical joint limits. Thus, both closures are in line with the desired ones. We will test the ability of the proposed design to present such behavior through accurate simulations in the next section, and experimentally in Section VI.

Fig. 7(a) and (b) shows two CAD views of SoftHand 2, with main components highlighted. The hand includes two MAXON DC-X 22 s 24 V motors, mounted on the back. We also included 86:1 gearboxes, characterized by 15 W of continuous output power. A single Dyneema tendon runs in the whole hand.

The motor positions are acquired using magnetic sensors from Austrian Microsystem. Two encoders are included for each motor, as depicted in Fig. 7(b). This choice is due to the necessity of having an absolute measurement of motor angles, robust to possible unexpected switching OFFof the electronics. The number of tics of the two encoders is selected to be coprime. The absolute angle is then derived integrating the two measurements through the Chinese remainder theorem [33].

The firmware is implemented on a custom electronic board, mounted on the bottom part of the hand. Its schematics are openly released, and they are available online as part of the Natural Machine Motion Initiative [34]. The implemented control algorithm is discussed in Section VI-A.

We designed the geometry of hand bottom part, to guarantee an easy connection with standard mechanical interfaces. It is worth noticing that, thanks to the proposed actuation principle, combined with the discussed mechanical design, SoftHand 2 is completely self-contained. Motors, electronics, and sensors are all on-board, and only the energy supply is external to the hand. This compact design allows the easy plug-and-play integration of the SoftHand 2 with robotic manipulators. Fig. 8(a) shows the integration of Pisa/IIT SoftHand 2 with a Kuka LWR. This was

(a) (b)

Fig. 8. Pisa/IIT SoftHand 2 presents a completely self-contained design, i.e., motors, sensors, and electronics are all on-board. This enables an easy integration in robotic manipulators. As an example, panel (a) shows SoftHand 2 mounted on Kuka LWR. Panel (b) shows instead the application of SoftHand 2 as a prosthesis. The hand is here integrated with a custom socket designed for sEMG prosthetics.

made possible by the introduction of just two custom elements: an ROS node and a 3-D printed flange (both available at [34]).

Another application enabled by the hand self-contained design is the prosthetic one [35]. A preliminary example is shown in Fig. 8(b), where the SoftHand 2 is integrated with a socket. The mechanical interface is a standard Ottobock Quick Disconnect Wrist. Two surface electromyographic sensors (sEMGs) are integrated in the socket. We used the on-board electronics to implement sEMG signal analysis and hand control. Future work will be devoted to the further evolution of the SoftHand 2 in the prosthetic direction, which is here presented just as a proof of concept.

V. SoftHand 2 Dynamic Model and Numerical Simulation

To achieve a more complete understanding of Pisa/IIT SoftHand 2 behavior, we develop in this section a numerical model, including hand specific details. We describe in the following the derivation of friction-related terms. The derivation of the other terms is reported in the appendices.

A. Friction Terms

In Section III, we modeled friction effects through a Coulomb-like model [26]. The simplicity of the model was instrumental for obtaining a closed-form solution. However, since the Pisa/IIT SoftHand 2 actuation system is based on friction exploitation, we consider here a more accurate, yet still computationally tractable, model of this effect. In this way, the analytical results can be tested in a realistic simulation environment. Such model also clarifies the dependence of the actuation from both the sliding s and its derivative $\dot{s}$, informing the control strategy, as it will be discussed in the next section.

Considering the tension balance in (10), we model here the tension loss $V(\cdot)$ as the sum of viscous and static friction. The viscous friction loss is a linear function of the tendon portion speed $v_i\, c_i$, where c_i is the viscous friction coefficient. For static friction, we make use of the model proposed in [36], which is able to combine good accuracy and limited computational costs. The main idea is to introduce a virtual angle z_j for each variable subjected to friction θ_j. These variables evolve according to the dynamic

$$z_j^+ = \begin{cases} \theta_j + \Delta_j^{\max} & \text{if} \quad \theta_j \leq z_j - \Delta_j^{\max} \\ \theta_j - \Delta_j^{\max} & \text{if} \quad \theta_j \geq z_j + \Delta_j^{\max} \\ z_j & \text{otherwise} \end{cases} \tag{37}$$

where θ_j is the angle describing the rotation of the jth pulley, z_j is the virtual angle at a certain time instant, and z_j^+ is its value in the subsequent instant. $\Delta_{\max}^j$ is the friction range. Friction force on the jth pulley is $(\theta_j - z_j)\,\kappa_j$, where κ_j takes into account the amount of friction. Note indeed that the maximum static friction torque at the jth pulley is $\Delta_{\max}^j\,\kappa_j$. Combing these friction models with (10), the resulting tension balance at the jth portion is

$$T_j = T_{j-1} - v_j \frac{c_j}{r_j^2} - (\theta_j - z_j)\frac{\kappa_j}{r_j^2} \tag{38}$$

or, in matrix form

$$MT + \Lambda v + \Sigma(\theta - z) + e\tau_M = 0 \tag{39}$$

where Σ and Λ collect $\frac{\kappa_j}{r_j^2}$ and $\frac{c_j}{r_j^2}$ terms. $\theta \in \mathbb{R}^{117}$ and $z \in \mathbb{R}^{117}$ are vectors collecting θ_j and z_j. Thus, by substituting the novel friction balance in (16), the following friction driven input field results:

$$D(\theta, z, \dot{q}, \dot{s}) = \mathfrak{R}^T\, M^{-1}\left(\Lambda\left(M^{-1}\mathfrak{R}\dot{q} - e_v\dot{s}\right) + \Sigma(\theta - z)\right) \tag{40}$$

where $\mathfrak{R}$ has the same role of $\bar{R}$ of (16), and it is derived in Appendix C. To complete the model, it remains to relate θ_i to joint angles. This can be done by combining $r_i\theta_i = \int v_i\, dt$, (14), and by dividing for pulley radii

$$\theta = N(M^{-1}\mathfrak{R}\, q - e_v s) \tag{41}$$

where N is the diagonal matrix having as ith diagonal element $\frac{1}{r_i}$. Combining with (40), it yields to

$$D(z, q, \dot{q}, s, \dot{s}) = \mathfrak{R}^T M^{-1}(\Lambda\left(M^{-1}\mathfrak{R}\dot{q} - e_v\dot{s}\right) + \Sigma(N(M^{-1}\mathfrak{R}q - e_v s) - z)). \tag{42}$$

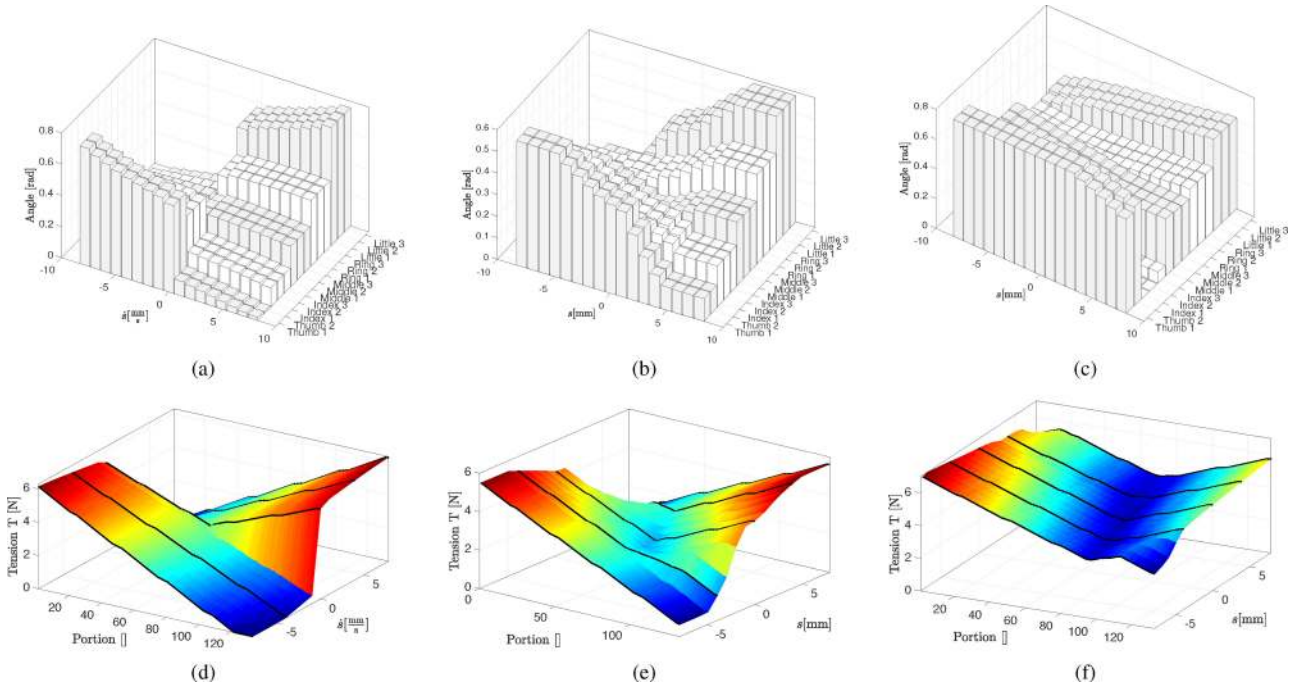

Fig. 9. Effect of sliding in the steady-state posture of SoftHand 2 [Panels (a, b, c)] and corresponding distributions of tension on the tendon [Panels (d, e, f)], according to the proposed model. A constant force $\tau_{\mathrm{M}} = 6\mathrm{N}$ is applied in all the cases. In panel (a, d), a constant sliding speed $\dot{s}$ is considered, which ranges from $-\frac{5\pi}{2}$ to $\frac{5\pi}{2}$ $\frac{\mathrm{mm}}{\mathrm{s}}$. The final postures and tensions are polarized among two limit configurations, in accordance to Section III. Panels (b, e) present instead the case of a constant sliding, i.e., s ranges from $-\frac{5\pi}{2}$ to $\frac{5\pi}{2}$ mm. In this case, postures and tensions change continuously from a limit posture to the other. Panels (c, d) report a simulation analogous to the previous one, but where a constant force of 2 N is applied to the fingertip of the index finger. In panels (a, b, c) abduction angles are omitted for the sake of clarity. Positive angles correspond to hand closure. In panels (d, e, f), the tensions corresponding to $\dot{s} \in \{-\frac{5\pi}{2}, -\frac{5\pi}{4}, 0, \frac{5\pi}{4}, \frac{5\pi}{2}\}\frac{\mathrm{mm}}{\mathrm{s}}$ and $s \in \{-\frac{5\pi}{2}, -\frac{5\pi}{4}, 0, \frac{5\pi}{4}, \frac{5\pi}{2}\}$mm are highlighted with black solid lines.

Thus, in presence of static friction (i.e., $\Sigma \neq \emptyset$), also a constant sliding (i.e., $s \neq 0$ and $\dot{s} \equiv 0$) can serve as an actuation. It is worth noticing that in accordance to the analytical model proposed in Section III, the input field $\mathfrak{R}^T M^{-1} \Lambda\, e_v$ is equal to R_{f}^T ($V_{\max}$ and Λ have identical structure). Similar considerations can be drawn for $\Sigma\, N\, M^{-1}\, e_v$. However, the dependency on z prevents from expressing the solution in closed form.

B. Overall Resulting Model

Including dynamics effects, a generic robotic system driven by augmented adaptive synergies can be modeled as

$$B(q)\ddot{q} + W(q,\dot{q})\dot{q} + \Gamma(q) = Q(q)u + J(q)^T f_{\mathrm{ext}} \qquad (43)$$

where z dynamics is (37), q are hand joint angles, with their derivatives $\dot{q}, \ddot{q}$. $B(q)$ is the inertia matrix. $W(q,\dot{q})$ collects centrifugal, Coriolis, and dissipative effects. $\Gamma(q)$ collects elastic forces. $J(q)^T f_{\mathrm{ext}}$ collects the torque action on joints as an effect of external forces. $u \triangleq \left[\tau_M \;\; s \;\; \dot{s}\right]^T$ collects inputs, $Q(q)$ is the transmission ratio from u to joint torques. In the case of the Pisa/IIT SoftHand 2, these terms can be expressed as

$$\begin{cases} W(q,\dot{q}) \triangleq C(q,\dot{q}) + F + \mathfrak{R}^T\, M^{-1}\, \Lambda \\ \Gamma(q) \triangleq G(q) - \mathfrak{R}^T\, M^{-1}\, \Sigma\, (N\, M^{-1}\, \mathfrak{R}\, q - z) \\ Q(q) \triangleq \mathfrak{R}^T\, M^{-1} \left[\, \frac{1}{2} M\, e_v \;\; \Sigma\, N\, e_v \;\; -\Lambda\, e_v \,\right] \\ u \triangleq \left[\tau_M \;\; s \;\; \dot{s}\right]^T \end{cases} \qquad (44)$$

where the derivation of $B(q)$ and $C(q,\dot{q})$ is described in Appendix A, the elastic field $G(q)$ is described in Appendix B, the transmission ratio $\mathfrak{R}$ is described in Appendix C. We consider friction on joint level as the linear function of the joint derivatives $F\,\dot{q}$, with $F \in \mathbb{R}^{19\times 19}$ diagonal. The remaining terms are friction-related terms introduced in Section V-A. The MATLAB code implementing the proposed model is available at the Natural Machine Motion Initiative web site [34].

C. Identification

As already discussed in previous sections, we fixed pulley radii r_i and spring stiffnesses k_i by design. Geometric dimensions are known too from the design, i.e., $R_i\ \beta$ in (46), $a\ b\ c\ d$ in (50), and phalanxes lengths in Appendix A. We also make the simplifying assumption for friction coefficients c_i, κ_i in (38), to be equal for each pulley. We estimate these values through an identification procedure. We also estimate abduction joint stiffnesses of (47). The data set was collected through *PhaseSpace* system,[1] an active led based motion capture system, with a sample time of 0.021 s and submillimeter precision. We placed a led on each phalanx and five on the back of the palm. We close for $five$ times by applying a constant force ($\tau_{\mathrm{M}} = 15$ N) and no sliding ($s = 0$). The data were filtered with a low-pass filter with two poles in -20 Hz. The identification was performed by

[1] http://www.phasespace.com/

searching for the model parameters, which generated in simulation a closing behavior as close as possible to the one measured. The considered distance measure was the 2-norm between the joint evolutions.

D. Simulative Results

Using the proposed identified model, we performed simulations to test predictions of the analytical model of Section III. According to the Augmented Adaptive Synergy framework, a sliding with constant velocity $\dot{s}$ can actuate the hand in a novel direction of actuation. Fig. 9(a) shows the final posture of SoftHand 2 when $\tau_{\mathrm{M}} = 6$ N, and $\dot{s}$ is constant with values ranging from $-\frac{5\pi}{2}$ to $\frac{5\pi}{2}\frac{\mathrm{mm}}{\mathrm{s}}$. Fig. 9(d) presents the corresponding tension distribution of the tendon. Results are in accord with indications of the theoretical model in Section IV, i.e., the constant sliding generates a tension redistribution, which produces a coordinated closure of ring and little, and opening of the thumb and index fingers, when $\dot{s} > 0$, and vice versa when $\dot{s} < 0$.

In Fig. 9(b), we report the results of an analogous simulation, where instead of constant $\dot{s}$, we consider a step variation of s with values ranging from $-\frac{5\pi}{2}$ to $\frac{5\pi}{2}\mathrm{mm}$. Fig. 9(e) presents corresponding tension distribution on tendon. Interestingly, the effect is similar to the constant sliding. However, these simulations demonstrate how, thanks to static friction, the entire range of postures between the two extremes can be achieved statically, using as control input s.

To conclude the analysis, we present an example of how an external force affects both hand posture [in Fig. 9(c)] and tension distribution [in Fig. 9(f)]. The input torque and sliding is the same as in the latter simulation, but we introduced here a 2 N constant force applied orthogonally to index fingertip. The most evident effect is, according to the introduced framework, that index finger remains almost completely straight (angles equal to zero), while the other fingers close more. The most affected finger is the thumb, which is near to the index and with lower inertia w.r.t. the middle, which instead closes slightly less. It is also interesting to note that the second DoA (i.e., the change of s) still generates a relative reconfiguration of the finger angles. Finally, note that, as expected, the force increases the tension in the tendon portion nearest to the index, i.e., approximately from portion 1 to portion 50.

VI. Experimental Validation

A. Control

From the simulations, it results that a step variation of the sliding s is as much effective as a step variation of sliding speed $\dot{s}$ in generating limit configurations, and while it appears more effective in generating intermediate ones. We thus consider here a simple control law defining motor torques, such that desired s and σ are achieved. Fig. 10 shows the block scheme. We map sliding s to the equivalent angle by divining for motor pulley radius r. The motor angles θ_1 and θ_2 are mapped into σ and s according to the definition, i.e., as semisum and semidifference. The control action is defined by an error-based PD control, with proportional gain equals to $0.2\frac{\mathrm{N}}{\mathrm{rad}}$ and $0.015\frac{\mathrm{N\,s}}{\mathrm{rad}}$ (heuristically tuned). The control is mapped back to motor inputs as semisum and semidifference.

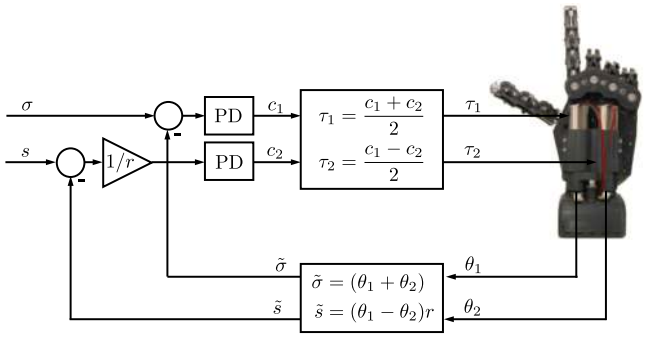

Fig. 10. Control architecture of Pisa/IIT SoftHand 2. Two proportional-integral controllers regulate the angles of the two motors. No measurement from the hand posture is required. The references are expressed as σ and s.

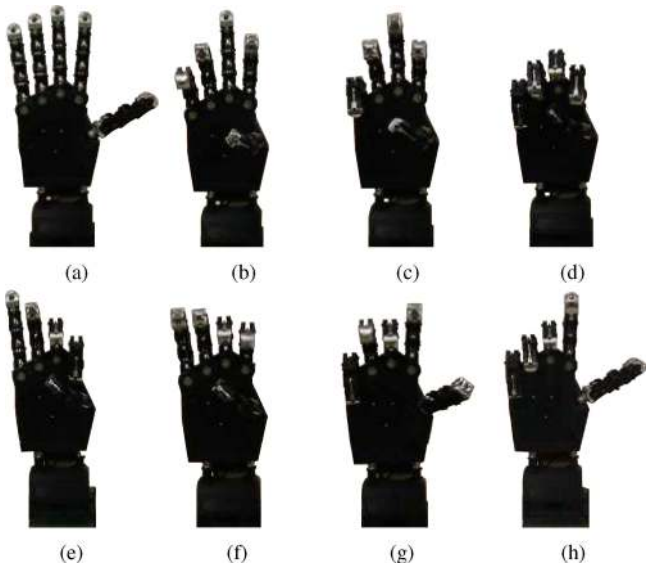

Fig. 11. Photosequences of the two movements corresponding to the two DoAs. The first degree (a, b, c, d) resembles the first synergy of grasp. It generates a coordinate opening-closing of all the fingers, and it can be used to establish firm grasps. The second degree (e, f, g, h) instead generates a reconfiguration of the relative posture of the fingers, and it can be used to execute more complex tasks. It resembles high-order synergies of grasping and manipulation. This DoA is driven by friction, and controlled through a sliding of the tendon.

Fig. 11 shows two photo sequences of SoftHand 2 movements obtained through the considered controller. In the first row $s = 0$, and σ moves from 0 to $\frac{\pi}{2}$. Thus, hand closes according to the first soft synergy, the same implemented in the original Pisa/IIT SoftHand [19]. In the second row, $\sigma = \frac{\pi}{2}$ and s moves from $\frac{5\pi}{2}$ to $-\frac{5\pi}{2}$mm. This is the movement that characterize SoftHand 2 w.r.t. the previous version, and that is completely conveyed by friction effects. Note that the behavior is coherent with the design framework (see Section IV) and with the one obtained in simulation (see Section V-D).

B. Human–Machine Interface

The SoftHand 2 can be controlled through a digital input by a computer. However, to realize a more natural control by a

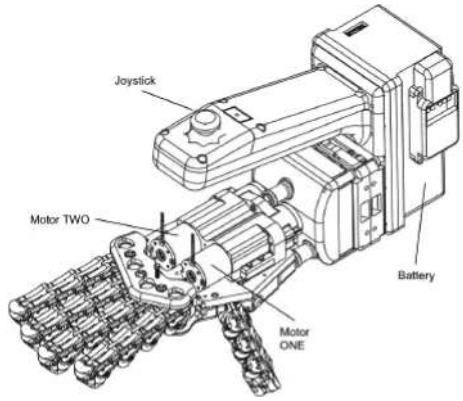

Fig. 12. Sketch of the SoftHand 2 human–machine interface. It enables an user to easily experiment with the robotic hand. The main subsystems are highlighted in figure. The interface includes a battery, the only component not already included on-board on the hand.

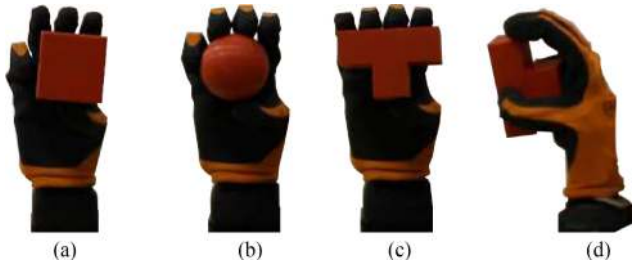

Fig. 13. Using the first DoA, Pisa/IIT SoftHand 2 establishes stable power grasps for all considered object shapes, with characteristics depending on the affordances of the object. (a) Cube. (b) Sphere. (c) Tetris. (d) Tetris.

Fig. 14. Comparison of grasping capabilities, between one DoA and two DoAs. The grasps (a) and (c) are obtained using the first DoA of the SoftHand 2. The second DoA enables more natural grasps when grasping small and/or flat objects, as with the banknote and the credit card in panels (b) and (d). (a) Banknote. (b) Banknote. (c) Card. (d) Card.

human operator, we designed a mechanical interface (see Fig. 12). The operator, holding the handle, can move a joystick (512 ADAFRUIT analog 2-axis joystick) using the thumb. Upward direction is translated into an increase of the σ command (i.e., first DOA), in an integral fashion. The downward direction corresponds to a decrease of σ instead. Left and right directions correspond to a similar change of s. Pressing the select button reset the hand to initial position. The handle also holds a battery pack in the lower part. Using the proposed interface, we were able to test the SoftHand 2 performances independently from automatic planning and control performances.

Fig. 15. Photosequences of tasks performed by SoftHand 2 mounted on a Kuka LWR. In (a, b, c) and (d, e, f), a same object is grasped from two different sides, achieving two different grasps. In (g, h, i), the robot performs a precision grasp, and in (j, k, l), it slides a paper through the use of the index finger.

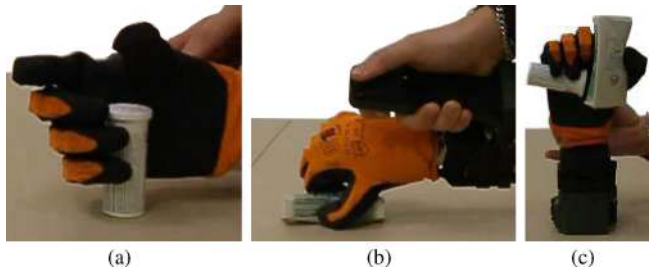

Fig. 16. Two distant objects are sequentially grasped by closing separately left and right sides of the hand.

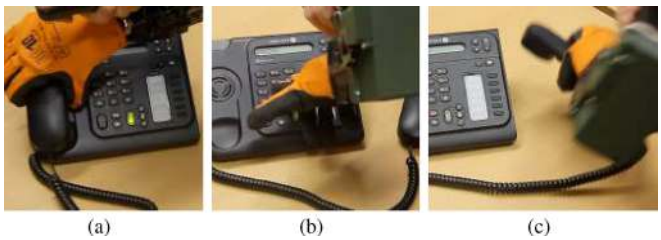

Fig. 17. SoftHand 2 grasps a receiver using both DoAs, and places it on the right-hand side of the phone. Then, the index finger is extended, and used to dial a number. Finally, the receiver is grasped as to use it.

Fig. 18. SoftHand 2 extracts a pen from its package, by relying on the preshaping ability provided by the second DoA.

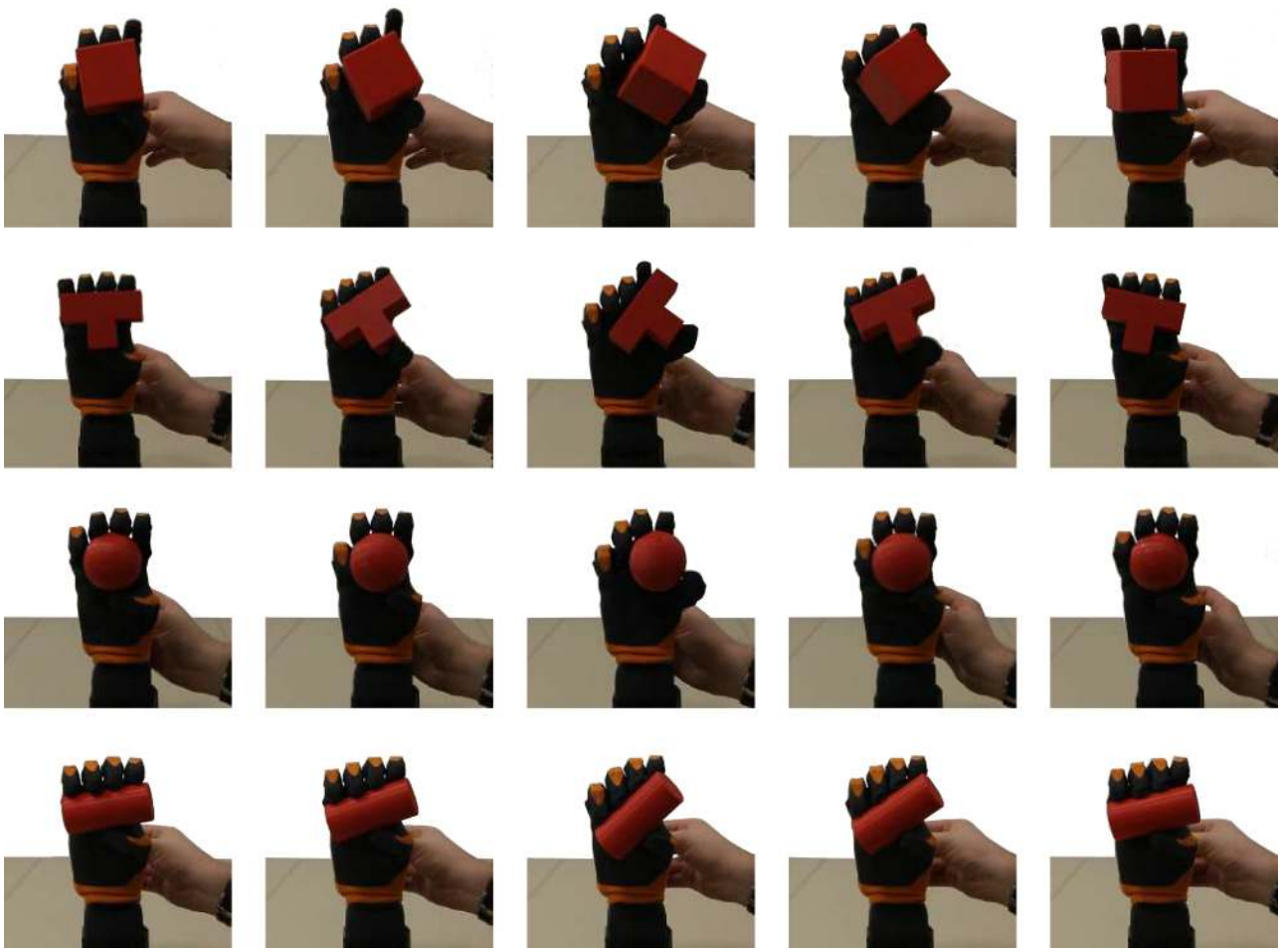

Fig. 19. Examples of in-hand manipulation. A same feedforward input allows to rotate objects with different shapes, relying on the intelligence embodied in the mechanism.

C. Experiments

The proposed actuation mechanism equips SoftHand 2 with various skills that we present here in several experiments. Using only the first degree of actuation σ and relying on hand adaptability, SoftHand 2 effectively performs different kinds of power grasps, as presented in Fig. 13. Note that different grasps are achieved even for the same object if grasped differently, as shown in panels (c, d). In Fig. 14, SoftHand 2 grasps two thin objects using the first DoA in panels (a, c). The grasp is correctly established, but power grasp is not fully coherent with the task (e.g., the banknote is stretched). In panel (b, d), the hand grasps the same objects using a combination of the two DoAs. Natural precision grasps are achieved in this case. As discussed above, the SoftHand 2 has a completely self-contained design, enabling easy integration with robotic manipulators. To show that, in Fig. 15, we mount Pisa/IIT SoftHand 2 on a Kuka LWR, and we perform tasks exploiting both DoAs. Panels (a, b, c, d, e, f) show two power grasps of a same object. Panels (g, h, i) show a pinch grasp. In (j, k, l), the robot performs a nonprehensile manipulation of a paper sheet using the extended index finger. In Fig. 16, the ability of closing separately the two parts of the hand is exploited to sequentially grasp two objects physically distant from each other. In Fig. 17, the operator grasps a receiver using the first DoA, and places it to the right-hand side of the phone. Then, he uses the second DoA to obtain a posture as in Fig. 11(h). Through the extended index, he dials a phone number. Finally, a power grasp is used to grasp again the receiver as to use it. In Fig. 18, SoftHand 2 extracts a pen from its

Fig. 20. Example of in-hand manipulation. We can use SoftHand 2 for opening a jar without main compensations on the wrist level.

Fig. 21. Example of in-hand manipulation. Following a feedforward input, SoftHand 2 pours coffee from a cup to another.

package by exploiting all the range of postures that the second DoA provides. It is worth noticing that these tasks are all intuitively accomplished by specifying in feedforward a value of σ and s. It is the intelligence embodied in the mechanics that provides the necessary mechanical adaptation to the environment and the objects to be grasped or manipulated.

In Fig. 19, we present SoftHand 2 in-hand manipulation skills. In all the examples, the object is grasped using the first DoA, and then manipulated through a feedforward input of ramp shape on the second DoA. This is done independently from the object shape and size. The hand shapes autonomously its posture and maintains the grasp during manipulation, without the need of additional reactive control. Moving to more complex daily living activities, we exploit the manipulation skills introduced by the second degree of actuation and the hand mechanical intelligence, in opening a jar in Fig. 20, and pouring some coffee from a cup in Fig. 21. Note that both tasks are performed without any compensation at the wrist level.

We point the reader to the video footage, which includes all the presented experiments, and additional demonstration material.

VII. Conclusion

In this paper, the complexity–dexterity tradeoff related to the design of multisynergistic compliant hands is faced by the introduction of a novel actuation principle, exploiting the friction inevitably encountered in tendon systems to turn it to advantage. We formalized this idea in a novel framework, called *augmented adaptive synergy framework*. From the application of this idea, we derived the design of the Pisa/IIT SoftHand 2, an anthropomorphic robotic hand, with two DoAs, and 19 DoFs. The physical parameters of the hand are designed so that its free motions reproduce the first synergy of grasp [25] and a reconfiguration of the fingers closely related to higher order synergies [31] [28] [29]. We also presented an accurate mathematical model of the robotic hand, to perform simulations, which corroborate the analytical model, and drive the controller design. We validated the prototype in several realistic conditions, both with the hand connected to a robotic manipulator and operated through a mechanical interface. Among the various abilities shown, the capacity of performing in-hand manipulation of objects of different sizes is of particular interest. Indeed, this is here obtained without the need of any feedback, and completely relying on the intelligence embodied in the hand mechanical structure. Future work will focus on the development of high level control and planning algorithms, which can take fully advantage from the demonstrated hand capabilities. We will also investigate the possibility of combining the proposed Augmented Adaptive Synergies, with Dynamic Synergies [37], to further increase the hand capabilities.

Appendix A: Hand Kinematics

Each one of the four long fingers of Pisa/IIT SoftHand 2 presents three *interphalangeal* joints and one *abduction* joint, as shown in Fig. 22. The abduction joint is a revolute joint, while interphalangeal joints are CORE joints [27]. They are kinematically equivalent to an RR arm, with a virtual (i.e., no inertia) intermediate link with an equality constraint between the two joint angles [see Fig. 23(a) and (b)]. Hence, the 4-joint robotic finger dynamics is equivalent to a 7R arm with standard kinematics, plus three equality constraints, which reduce the DoFs to 4. This model describes index, middle, ring, and little fingers of the Pisa/IIT SoftHand. The thumb differs slightly, since it has one phalanx less and the abduction axis is oriented differently (see Fig. 7).

Appendix B: Joint Impedance

Fig. 24 shows a schematic representation of interphalangeal elastic mechanism. The spring characteristic is considered

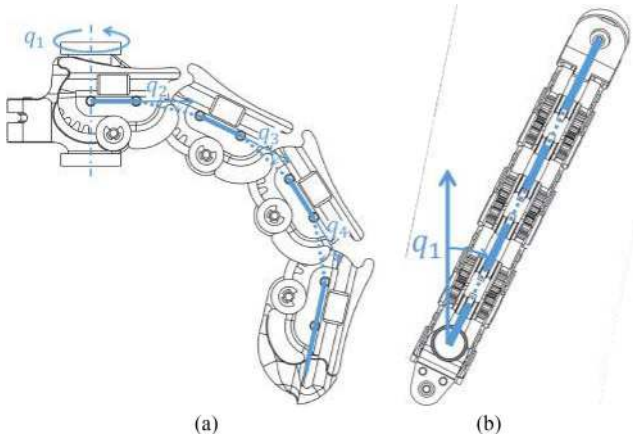

Fig. 22. Finger of Pisa/IIT SoftHand 2. It can be kinematically described as a 7R arm with three equality constrains, resulting in a 4-DoFs model. (a) Side view. (b) Top view.

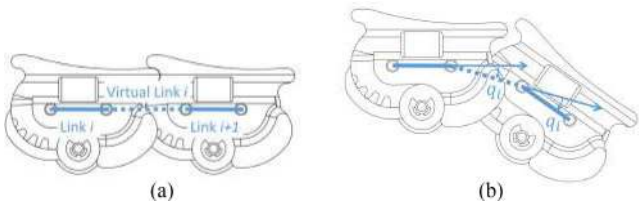

Fig. 23. Interphalangeal joint is a realization of a *CORE joint*. We model it as an RR arm, with a virtual (i.e., no inertia) intermediate link. The pure revolute constraint between the two phalanxes translates into an equality constraint between the two angles of the arm. (a) Rest position. (b) Flexed position.

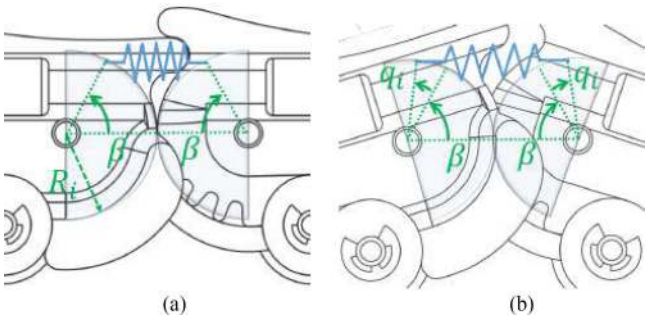

Fig. 24. Schematic representation of the interphalangeal spring system, in rest (a) and flexed (b) positions. q_i is the joint angle, β is the angle of the spring connection with respect to the horizontal, and R_i is the envelope radium. (a) Rest position. (b) Flexed position.

linear. The spring deflection w.r.t. q_i is $2R_i(\cos(\beta_i + q_i) - \cos(\beta_i))$. Gear envelope radius R_i is considered constant. The angle of the spring connection with respect to the segment connecting the envelope centers is referred as β_i. Resulting spring energy is

$$E(q) = \sum_{i=2}^{4} 2k_i R_i^2 (\cos(\beta_i + q_i) - \cos(\beta_i))^2 . \quad (45)$$

The interphalangeal elastic field $G_i(q)$ is

$$G_i(q) = 4\, k_i\, R_i^2 (\cos(\beta_i) - \cos(\beta_i + q_i)) \sin(\beta_i + q_i). \quad (46)$$

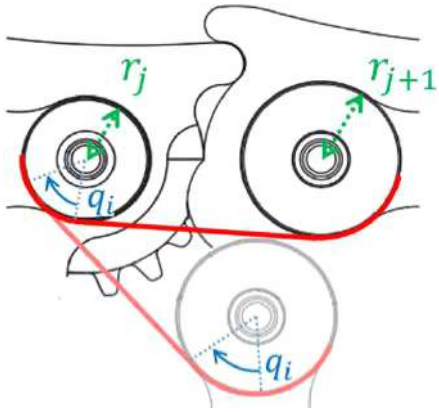

Fig. 25. Schematic representation of interphalangeal actuation system, in its rest and flexed positions. The red lines represent the tendon. Hand closure is associated to a reduction of tendon length proportional to the radii of pulleys actuating the joint.

The abduction elastic mechanism is modeled as a torsional linear spring

$$G_1(q) = k_1 (q_1 - \bar{q}) \quad (47)$$

where $\bar{q}$ is abduction joint rest position.

Appendix C: Transmission Ratio

Fig. 25 presents the left side of the interphalangeal joint actuation system. The variation of tendon length due to the closure of ith joint $l_i(q)$ is $(r_j + r_{j+1})q_i$, where r_j, r_{j+1} are radii of the pulleys acting on the ith joint left side. Hence, from kineto–static relationship, the torque on the ith joint due to the left side of the mechanism is equal to $(r_j + r_{j+1})T_j$. Total torque is obtained adding up right and left sides

$$\tau_i = (r_j + r_{j+1})T_j + (r_k + r_{k+1})T_k \quad (48)$$

where τ_i is the total torque acting on the joint, and r_k, r_{k+1} are the radii of the two pulleys acting on the ith joint right side. Note that other tendon configurations are possible, as shown in Fig. 26, with transmission ratio: 1) $r_j + r_{j+1}$, 2) $r_j - r_{j+1}$, 3) $-r_j + r_{j+1}$, 4) $-r_j - r_{j+1}$. This introduces an addition DoF in the mechanical design that we do not further discuss further for the sake of space.

A different structure is used to actuate the abduction joint. Fig. 27 shows the mechanism in various configurations, with significant quantities highlighted. We refer to $l_l(q_1)$ and $l_r(q_1)$ as the lengths of the left and right portions of the tendon. q_1 is the abduction angle.

Here, we neglect variations of $l_1(q_1)$ and $l_2(q_1)$ associated with changes of the tendon tangency point. Joint torques depend on left-hand and right-hand side tension T_L, T_R through two different transmission ratios, $X(q_1) \triangleq [\frac{\partial l_1(q_1)}{\partial q_1}, \frac{\partial l_2(q_1)}{\partial q_1}]$. Thanks to the symmetry of the mechanism w.r.t. q_1, we consider only configurations (a–b) in Fig. 27, i.e., $q_1 \geq 0$. The results are extended for $q_1 < 0$, substituting $|q_1|$ to q_1, and inverting the order of the two terms.

There is a range of values of q_1 for which there is no contact between the central pulley [i.e., the one of radius e in Fig. 27(d)]

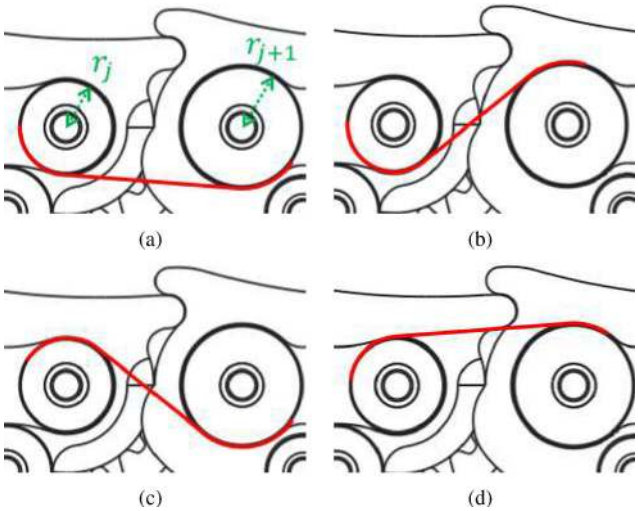

Fig. 26. Tendon configurations in interphalangeal actuation system. The red lines represent the tendon. Each configuration enables to implement a different, even negative, transfer ratio.

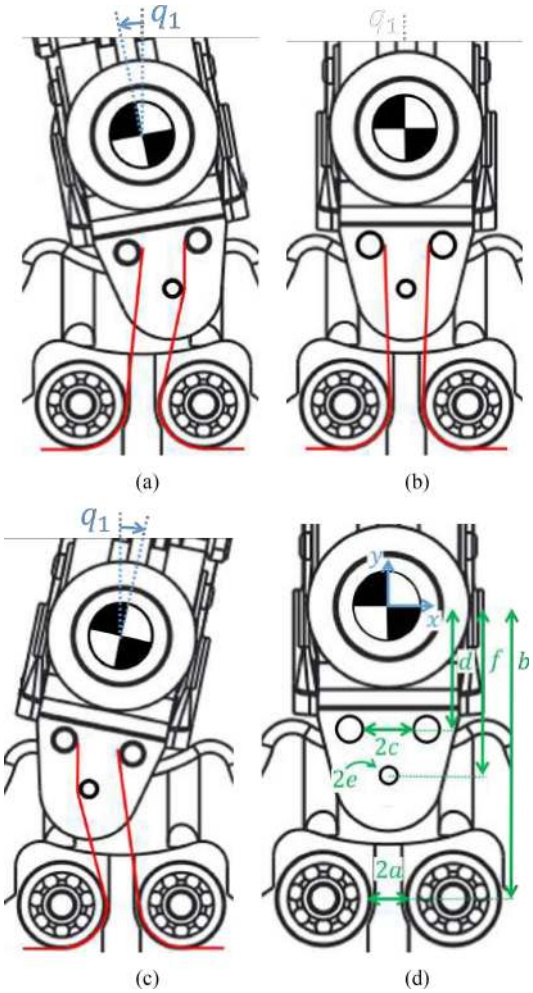

Fig. 27. Actuation system of the abduction joint. In (a–c), we present the joint in different configurations, the red lines represent the tendon. In (d), we highlight significant quantities, needed to derive the tendon length. (a) $q1 > 0$. (b) $q1 = 0$. (c) $q1 < 0$. (d) Significant quantities.

and the tendon. Outside the interval the transmission geometry changes. Thus, derivation of $l_1(q_1)$ and $l_2(q_1)$ has to be done separately for both cases. Transmission ratio is

$$X(q_1) \triangleq \begin{cases} X^-(q_1), & \text{if } q_1 \leq q_{\text{contact}} \\ X^+(q_1), & \text{if } q_1 > q_{\text{contact}} \end{cases} \tag{49}$$

where X^-, X^+ are transmission ratio in *no contact* and *contact* case, and $q_{\text{contact}} = \min\{q^* \in [0, \frac{\pi}{2}] \text{ s.t.: } X^-(q^*) = X^+(q^*)\}$. Simple geometrical considerations (see Fig. 27) bring to the following expressions for tendon lengths:

$$\begin{aligned} l_1(q_1) &= \left\| \begin{bmatrix} -a \\ -b \end{bmatrix} - R_{q_1} \begin{bmatrix} -c \\ -d \end{bmatrix} \right\| \\ l_2^-(q_1) &= \left\| \begin{bmatrix} a \\ -b \end{bmatrix} - R_{q_1} \begin{bmatrix} c \\ -d \end{bmatrix} \right\| \\ l_2^+(q_1) &= \left\| \begin{bmatrix} a \\ -b \end{bmatrix} - R_{q_1} \begin{bmatrix} e \\ -f \end{bmatrix} \right\| + \left\| \begin{bmatrix} c-e \\ f-d \end{bmatrix} \right\| \end{aligned} \tag{50}$$

where $||\cdot||$ is the Euclidean norm, and R_{q_1} is the clockwise rotation matrix of an angle q_1. We obtain $X(q)$ from (49) by deriving (50). $X(q)$, together with (48), specifies completely matrix $\mathfrak{R}$.

ACKNOWLEDGMENT

The authors would like to thank A. Brando, A. Di Basco, M. Maimeri, A. Raugi, and G. Santaera for their valuable support in the development and validation of the prototype.

REFERENCES

[1] A. Kochan, "Shadow delivers first hand," *Ind. Robot: Int. J.*, vol. 32, no. 1, pp. 15–16, 2005.
[2] M. Grebenstein *et al.*, "The DLR hand arm system," in *Proc. IEEE Int. Conf. Robot. Autom.*, 2011, pp. 3175–3182.
[3] Z. Xu and E. Todorov, "Design of a highly biomimetic anthropomorphic robotic hand towards artificial limb regeneration," in *Proc. IEEE Int. Conf. Robot. Autom.*, 2016, pp. 3485–3492.
[4] M. Zaremsky, L. E. Weiss, and T. A. Mutschler, "Servo robot gripper," Apr. 1 1986, US Patent 4, 579, 380.
[5] S. Montambault and C. M. Gosselin, "Analysis of underactuated mechanical grippers," *J. Mech. Design*, vol. 123, no. 3, pp. 367–374, 2001.
[6] A. M. Dollar and R. D. Howe, "The highly adaptive SDM hand: Design and performance evaluation," *Int. J. Robot. Res.*, vol. 29, no. 5, pp. 585–597, 2010.
[7] G. Smit, R. M. Bongers, C. K. Van der Sluis, and D. H. Plettenburg, "Efficiency of voluntary opening hand and hook prosthetic devices, 24 years of development?" *J. Rehabil. Res. Develop.*, vol. 49, no. 4, pp. 523–534, 2012.
[8] L. Birglen, C. M. Gosselin, and T. Laliberté, *Underactuated Robotic Hands*, vol. 40. New York, NY, USA: Springer, 2008.
[9] L. Zollo, S. Roccella, E. Guglielmelli, M. C. Carrozza, and P. Dario, "Biomechatronic design and control of an anthropomorphic artificial hand for prosthetic and robotic applications," *IEEE/ASME Trans. Mech.*, vol. 12, no. 4, pp. 418–429, Aug. 2007.
[10] T. Laliberté, M. Baril, F. Guay, and C. Gosselin, "Towards the design of a prosthetic underactuated hand," *Mech. Sci.*, vol. 1, no. 1, pp. 19–26, 2010.
[11] L. U. Odhner *et al.*, "A compliant, underactuated hand for robust manipulation," *Int. J. Robot. Res.*, vol. 33, no. 5, pp. 736–752, 2014.
[12] R. Deimel and O. Brock, "A novel type of compliant and underactuated robotic hand for dexterous grasping," *Int. J. Robot. Res.*, vol. 35, nos. 1–3, pp. 161–185, 2015.
[13] N. Feng, Q. Shi, H. Wang, J. Gong, C. Liu, and Z. Lu, "A soft robotic hand: Design, analysis, sEMG control, and experiment," *Int. J. Adv. Manuf. Technol.*, pp. 1–15, Mar. 2018, doi: 10.1007/s00170-018-1949-2.

[14] M. Santello, G. Baud-Bovy, and H. Jörntell, "Neural bases of hand synergies," *Frontiers Comput. Neurosci.*, vol. 7, 2013, Art. no. 23.

[15] M. Ciocarlie, C. Goldfeder, and P. Allen, "Dexterous grasping via eigengrasps: A low-dimensional approach to a high-complexity problem," in *Proc. Robot.: Sci. Syst. Manipulation Workshop—Sens. Adapting Real World*, Atlana, GA, USA, Jun. 2007, pp. 3270–3275.

[16] C. Y. Brown and H. H. Asada, "Inter-finger coordination and postural synergies in robot hands via mechanical implementation of principal components analysis," in *Proc. IEEE/RSJ Int. Conf. Intell. Robots Syst.*, 2007, pp. 2877–2882.

[17] A. Bicchi, M. Gabiccini, and M. Santello, "Modelling natural and artificial hands with synergies," *Philosoph. Trans. Roy. Soc. B: Biol. Sci.*, vol. 366, no. 1581, pp. 3153–3161, 2011.

[18] G. Grioli, M. Catalano, E. Silvestro, S. Tono, and A. Bicchi, "Adaptive synergies: An approach to the design of under-actuated robotic hands," in *Proc. IEEE/RSJ Int. Conf. Intell. Robots Syst.*, 2012, pp. 1251–1256.

[19] M. G. Catalano, G. Grioli, E. Farnioli, A. Serio, C. Piazza, and A. Bicchi, "Adaptive synergies for the design and control of the pisa/iit softhand," *Int. J. Robot. Res.*, vol. 33, no. 5, pp. 768–782, 2014.

[20] Z. Li, P. Hsu, and S. Sastry, "Grasping and coordinated manipulation by a multifingered robot hand," *Int. J. Robot. Res.*, vol. 8, no. 4, pp. 33–50, 1989.

[21] V. Kumar, E. Todorov, and S. Levine, "Optimal control with learned local models: Application to dexterous manipulation," in *Proc. IEEE Int. Conf. Robot. Autom.*, 2016, pp. 378–383.

[22] J. Shi, J. Z. Woodruff, P. B. Umbanhowar, and K. M. Lynch, "Dynamic in-hand sliding manipulation," *IEEE Trans. Robot.*, vol. 33, no. 4, pp. 778–795, Aug. 2017.

[23] H. Yousef, M. Boukallel, and K. Althoefer, "Tactile sensing for dexterous in-hand manipulation in roboticsa review," *Sens. Actuators A: Physical*, vol. 167, no. 2, pp. 171–187, 2011.

[24] C. Della Santina, G. Grioli, M. Catalano, A. Brando, and A. Bicchi, "Dexterity augmentation on a synergistic hand: The pisa/iit softhand+," in *Proc. IEEE-RAS 15th Int. Conf. Humanoid Robots*, 2015, pp. 497–503.

[25] M. Santello, M. Flanders, and J. F. Soechting, "Postural hand synergies for tool use," *J. Neurosci.*, vol. 18, no. 23, pp. 10105–10115, 1998.

[26] S. Andersson, A. Söderberg, and S. Björklund, "Friction models for sliding dry, boundary and mixed lubricated contacts," *Tribology Int.*, vol. 40, no. 4, pp. 580–587, 2007.

[27] J. R. Cannon and L. L. Howell, "A compliant contact-aided revolute joint," *Mechanism Mach. Theory*, vol. 40, no. 11, pp. 1273–1293, 2005.

[28] P. H. Thakur, A. J. Bastian, and S. S. Hsiao, "Multidigit movement synergies of the human hand in an unconstrained haptic exploration task," *J. Neurosci.*, vol. 28, no. 6, pp. 1271–1281, 2008.

[29] C. Della Santina *et al.*, "Postural hand synergies during environmental constraint exploitation," *Frontiers Neurorobotics*, vol. 11, 2017, Art. no. 41.

[30] M. Gabiccini, G. Stillfried, H. Marino, and M. Bianchi, "A data-driven kinematic model of the human hand with soft-tissue artifact compensation mechanism for grasp synergy analysis," in *Proc. IEEE/RSJ Int. Conf. Intell. Robots Syst.*, 2013, pp. 3738–3745.

[31] E. Todorov and Z. Ghahramani, "Analysis of the synergies underlying complex hand manipulation," in *Proc. 26th Annu. Int. Conf. IEEE Eng. Med. Biol. Soc.*, 2004, vol. 2, pp. 4637–4640.

[32] "Sapporo high precision ball bearings datasheet," [Online]. Available: http://www.sppc.co.jp/eng/download/index.html. accessed on: Sep. 2017.

[33] P. Duchet, "Hypergraphs," in *Handbook of Combinatorics*, vol. 1. Cambridge, MA, USA: MIT Press, 1996, pp. 381–432.

[34] C. Della Santina *et al.*, "The quest for natural machine motion: An open platform to fast-prototyping articulated soft robots," *IEEE Robot. Autom. Mag.*, vol. 24, no. 1, pp. 48–56, Mar. 2017.

[35] M. Rossi, C. Della Santina, C. Piazza, G. Grioli, M. Catalano, and A. Biechi, "Preliminary results toward a naturally controlled multisynergistic prosthetic hand," in *Proc. Int. Conf. Rehabil. Robot..*, 2017, pp. 1356–1363.

[36] V. Hayward and B. Armstrong, "A new computational model of friction applied to haptic rendering," in *Proc. Experimental Robot. VI*, 2000, pp. 403–412.

[37] C. Piazza, C. Della Santina, M. Catalano, G. Grioli, M. Garabini, and A. Bicchi, "Softhand pro-d: Matching dynamic content of natural user commands with hand embodiment for enhanced prosthesis control," in *Proc. IEEE Int. Conf. Robot. Autom.*, 2016, pp. 3516–3523.

Cosimo Della Santina received the B.S. degree *cum laude* in computer engineering and the M.S. degree *cum laude* in automation and robotics engineering from University of Pisa, Pisa, Italy. He is currently working toward the Ph.D. degree in robotics with Research Center E. Piaggio, University of Pisa.

His main research interests include model-based design, sensing, and control of soft robots and soft hands.

Cristina Piazza received the B.S. degree in biomedical engineering and the M.S. degree in automation and robotics engineering from University of Pisa, Pisa, Italy. She is currently working toward the Ph.D. degree in robotics with Research Center E. Piaggio, University of Pisa.

Her main research interests include the design of soft artificial hands for robotic and prosthetic applications.

Giorgio Grioli received the Ph.D. degree in robotics, automation, and engineering from University of Pisa, Pisa, Italy, in 2011.

He is a Researcher with the Italian Institute of Technology, where he investigates design, modeling, and control of soft robotic systems applied to the augmentation of, rehabilitation of, and interaction with the human. He is the author of more than 60 articles (both journal papers and conference proceedings) in the fields of soft robotic actuation, robot hand design, and haptics.

Dr. Grioli serves as an Associated Editor for ICRA and ICORR and is currently co-editing a special issue of *Actuators* on "Variable Stiffness and Variable Impedance Actuators."

Manuel G. Catalano (M'13) received the B.S. and M.S. degrees in mechanical engineering and the Ph.D. degree in robotics from Università di Pisa, Pisa, Italy, in 2006, 2008, and 2013, respectively.

He is currently a Researcher with the Italian Institute of Technology and a Collaborator of Centro di Ricerca E. Piaggio, University of Pisa. His main research interests include the design of soft robotic systems, human robot interaction, and prosthetics.

Dr. Catalano won the Georges Giralt Ph.D. Award in 2014, the prestigious annual European award given for the best Ph.D. thesis by euRobotics AISBL.

Antonio Bicchi (F'05) received the Laurea degree *(cum laude)* in mechanical engineering from Universitá di Pisa in 1984 and the Ph.D. degree in mechanical engineering from Università di Bologna, Bologna, Italy, in 1989. He was a Visiting Scholar of Artificial Intelligence Laboratory, Massachusetts Institute of Technology, Cambridge, MA, USA, in 1989.

He is a Professor of automatic control with the Department of Information Engineering and Centro E. Piaggio, University of Pisa, where he has been leading the Robotics Research Group since 1990. Since 2009, he has also been a Senior Researcher with the Italian Institute of Technology, Genoa, Italy, where he leads the Soft Robotics for Human Cooperation and Rehabilitation Research Line. His main research interests include the field of robotics, haptics, and automatic control. He has published more than 400 papers on international journals, books, and refereed conferences.

Mr. Bicchi has been granted an ERC Advanced Grant in 2011.